Seras-Franzoso, J.; Steurer, C.; Roldan, M.; Vendrell, M.; Vidaurre-Agut, C.; Tarruella, A.; Saldana, L.... (10-1). Functionalization of 3D scaffolds with protein-releasing biomaterials for intracellular delivery. Journal of Controlled Release. 171(1):63-72. https://doi.org/10.1016/j.jconrel.2013.06.034

Ms. Ref. No.: JCR-D-13-00225 (REVISED VERSION)

Functionalization of 3D scaffolds with protein-releasing biomaterials for intracellular delivery.

Joaquin Seras-Franzoso [1, 2, 3], Christoph Steuer [1], Mònica Roldán [4], Meritxell Vendrell [4], Carla Vidaurre-Agut [5], Anna Tarruella [4], Laura Saldaña [3, 6], Nuria Vilaboa [3,6], Marc Parera [3,7], Elisa Elizondo [3,7], Imma Ratera [3,7], Nora Ventosa [3,7], Jaume Veciana [3,7], Alberto J. Campillo-Fernández [5], Elena García-Fruitós [3, 1, 2], Esther Vázquez [1, 2, 3 *], Antonio Villaverde [1, 2, 3 *]

[1] Institut de Biotecnologia i de Biomedicina, Universitat Autònoma de Barcelona, Bellaterra, 08193 Barcelona, Spain

[2] Department de Genètica i de Microbiologia, Universitat Autònoma de Barcelona, Bellaterra, 08193 Barcelona, Spain

[3] CIBER de Bioingeniería, Biomateriales y Nanomedicina (CIBER-BBN), Zaragoza, Spain

[4] Servei de Microscòpia, Universitat Autònoma de Barcelona, Bellaterra 08193 Barcelona, Spain

[5] Metis Biomaterials S.L., Avda. Benjamin Franklin, 12, CEEI Valencia, 46980 Paterna, Spain

[6] Hospital Universitario La Paz-IdiPAZ, Paseo de la Castellana 261, 28046 Madrid, Spain

[7] Department of Molecular Nanoscience and Organic Materials, Institut de Ciencia de Materials de Barcelona (CSIC), Bellaterra, 08193 Barcelona, Spain

***** Corresponding authors:

Esther Vázquez; esther.vazquez@uab.cat; A. Villaverde; antoni.villaverde@uab.cat

Abstract

Appropriate combinations of mechanical and biological stimuli are required to promote proper colonization of substrate materials in regenerative medicine. In this context, 3D scaffolds formed by compatible and biodegradable materials are under continuous development in an attempt to mimic the extracellular environment of mammalian cells. We have here explored how novel 3D porous scaffolds constructed by polylactic acid, polycaprolactone or chitosan can be decorated with bacterial inclusion bodies, submicron protein particles formed by releasable functional proteins. A dipping-based decoration method specifically favors the penetration of the functional particles up to 300 μm from the materials' surface. The functionalized surfaces supports the intracellular delivery of biologically active proteins to up to more than 80 % of the colonizing cells, a process that is slightly influenced by the chemical nature of the scaffold. The combination of 3D soft scaffolds and protein-based sustained release systems (bioscaffolds) offers promise in the fabrication of bio-inspired hybrid matrices for multifactorial control of cell proliferation in tissue engineering under complex architectonic setting-ups.

Keywords: Nanoparticles; 3D scaffolds; polylactic acid (PLA); bottom-up delivery; bioscaffold; tissue engineering

Background

Regenerative medicine pursues the reconstruction of damaged tissues by the controlled growth of cells, either in vitro followed by implantation or directly in vivo. As a pivotal concept supporting this approach, cells must be cultured on biocompatible substrates that should ideally provide the right combination of mechanical and biological stimuli for colonization, proliferation and, eventually, for differentiation [1,2]. Reaching an appropriate spatial distribution of cells would be in general convenient, but it is specifically demanded in the case of tissues formed by heterogeneous mixtures of cell types. The use of metal nanoparticles and magnetic force is of special interest as it permits a fine control and volumetric distribution of diverse cell lineages in architectonically complex organic structures [3]. More generally, 3D scaffolds are under development to provide cell friendly substrates for cell attachment and proliferation, mimicking the intercellular matrix and the natural cell environment more efficiently than the conventional 2D surfaces used in plain cell culture. Apart from metals, ceramics, protein-based hydrogels and carbon nanotubes, a spectrum of biocompatible and biodegradable polymers is being explored for 3D culture useful ex vivo and for implantation, including hyaluronic acid (HA), polylactic acid (PLA), polyglycolic acid (PLGA), chitosan (CHT), polycaprolactone (PCL), polyanhidrides, polyorthoesters and dendrimers [2,4-6]. Controlling the material's architecture during biofabrication permits to define porosity for mass transfer and proper colonization of the inner surfaces [7]. In addition, 3D scaffolds are expected to offer unordered mechanical stimuli for mechano-transduction events [8], required for a fine control of cell response [9], more efficiently than 2D substrates. Ideally, mechanical stimulation should act synergistically with biological signals, among which soluble protein factors such as insulin-like growth factor I [10], nerve growth factor β [11,12], epidermal growth factor [13], osteoprotegerin [14], fibroblast growth factors [15], and vascular endothelial growth factor [15] are the most effective. While being naturally available in vivo, they must be externally supplied in ex vivo cell culture.

In the last years, bacterial inclusion bodies (IBs) have been revealed as adhesive but mechanically stable protein materials [16], that being fully biocompatible can be used to favor cell colonization and proliferation when used to decorate flat surfaces [17-20]. In addition, as functional biomimetics of hormone secretion granules [21-23], bacterial IBs penetrate mammalian cell membranes and release their forming protein for a therapeutic effect, when exposed to cultured target cells in form of Nanopills [24-26] (top-down) or as Bioscafolds [27] (bottom-up). In the last case, the IB-embedded protein results available intracellularly and extracelularly, what expands the diversity of situations under which this platform could be applied, The rational for the sustained protein release is a sponge-like amyloid organization in which releasable functional protein is embedded in non-toxic amyloid fibril networks [22]. In this study, we have determined how IBs can be used to functionalize 3D scaffolds formed by several promising biomaterials, and at which extent, the functional protein carried by IBs could be released and become available to mammalian cells in 3D architectonic settings with more applicability than 2D surfaces for in vivo regenerative medicine purposes.

Materials and methods

IB production and purification

Reporter IBs were formed by a variant of EGFP (VP1GFP), that when synthesized in bacteria self-organize as mechanically stable and highly fluorescent sub-micron particles [20]. These materials were produced in *Escherichia coli* JGT4 ($ClpA^-$; *clpA::kan, araD139* (*argF-lac*) U169 *rpsL150 relA1 flbB5301 deoC1 ptsF25* Rbs^R, Sm^R) [28] in which VP1GFP IBs resulted highly fluorescent [29]. Protein production and IB purification were done under standard protocols [24,30]. Briefly *E. coli* cultures were performed in shake flasks in Luria Bertani (LB) medium at 37 °C 250 rpm till reach an optical density at 550 nm (OD_{550}) of 0.5. At this point, 1 mM IPTG was added as gene expression inducer. Bacterial cultures were further cultured for 3 h at 37 °C and 250 rpm. The enzymatic digestion of the bacterial cell wall was carried out by lysozyme at 1 µg/ml for 2 h at 37C at 250 rpm in the same culture medium. Weakened bacteria were disrupted by several freeze/thaw cycles to the samples. IB samples were then extensively washed with 0.4 % Triton X-100 (v/v) for 1 h at room temperature and with 0.025 % NP40 (v/v), for 1 h at 4 °C, and treated with DNAse (at 0.6 µg/ml) for 1h at 37 °C to remove any potential contaminant DNA.

IB protein amount was determined through the Quantity One software, on Western blots for GFP immunodetection, using a GFP standard curve.

Materials

Scaffolds fabricated with CHT, PCL and PLA were supplied by Metis Biomaterials SL, Valencia (Spain), in form of 1.2 mm thickness and 7.5 mm diameter discs, to be used in 48-multiwell plates. PCL (Mw = 48,000) was purchased from Polysciences, PLA (Mw = 124,000) was purchased from Cargill-Dow and CHT was purchased from Novamatrix (Protasan UP B 80-20). CHT samples (commercial reference: CHT MW48) were prepared by freeze-gelation obtaining a global porosity of 90 % and a mean pore size of 150 µm. Internal morphology of CHT samples mimic a honeycomb structure. PCL

(commercial reference: PCL MW48/12) and PLA (commercial reference: PLA MW48/12) scaffolds were prepared by freeze-extraction obtaining a global porosity of 70 % and a mean pore size of 150 µm. In both cases, pores were interconnected (Figure 1). Pore sizes and interconnections were determined by direct measurement using SEM micrographs obtained from different samples. For roughness analyises of the scaffolds, samples were coated with chromium. Surface studies images were taken with a 3D Optical Surface Metrology System Leica DCM 3D microscope (Leica Microsystems) using the 10 x objective.

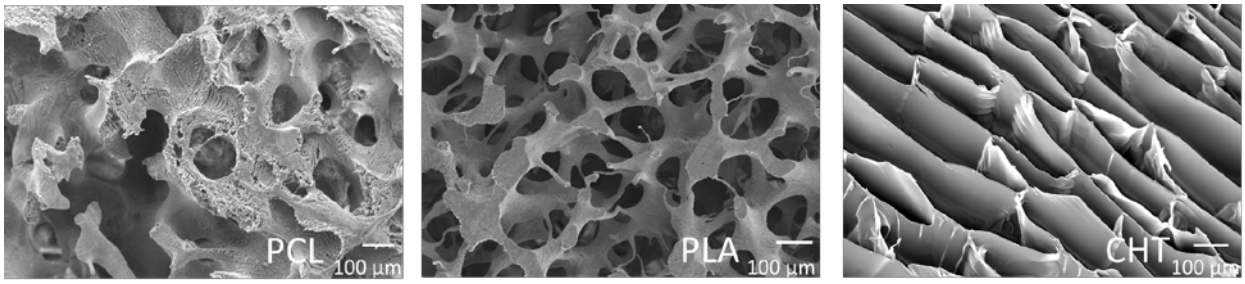

Figure 1. Micro-architecture of the 3D biomaterials used in this study.

Scaffold decoration

3D scaffolds (Metis Biomaterials) were washed three times in PBS for 5 min at room temperature and incubated in ethanol 70 % overnight at 4°C to inactivate possible contaminants. Then, scaffolds were washed again three times in PBS for 5 min at room temperature. Three distinct procedures were implemented to decorate the scaffolds with IBs.

Injection – IBs resuspended in 0.1 mL PBS (40 µg/ mL final concentration) were injected manually in the middle of the scaffold with 1 ml syringe through a 0,8 mm diameter needle. Note that IB adsorption to the material necessarily implies the contact between the particle and the material surface. In this regard, the flow applied by injection seems to hinder this contact in the centre of the scaffold, sweeping along most

of the IBs towards more external sections of the scaffolds where the injection flow reduces its strength.

Dripping – 0.1 mL of the IB suspension (40 µg/ mL final concentration) were added drop by drop onto the scaffold surface.

Dipping – Scaffolds were placed into 5 mL tubes and incubated in 4 mL of IB suspension (40 µg/ mL final concentration) overnight at 4°C under gentle rotation to favour the contact between IB in suspension and the scaffold. The higher solution volume permits to guarantee that the scaffolds are completely submerged, and under this IB excess we assume saturating concentrations on the three methods (note that in Injection and Dripping all the IB material is in direct contact with the scaffolds).

After IB decoration, scaffolds were washed in PBS for 5 min at room temperature. All the procedures were carried out under sterility conditions.

Mammalian cell culture and IB Internalization assay

HeLa cells (human cervical adenocarcinoma ATCC CCL-2) and 1BR3.G (human skin fibroblasts) cells were routinely maintained in α-MEM supplemented with 10 % (v/v) fetal bovine serum and 2 mM L-glutamine in a humidified incubator at 37°C and 5% CO_2. $2 \cdot 10^5$ HeLa cells suspended in culture medium were seeded by the injection of 0.1 mL ($2 \cdot 10^6$ cells/ mL), into the middle of the scaffolds. Samples were then transferred to 24 well plates and cultured for 24 h in a humidified incubator, at 37°C and 5 % CO_2. Internalization of IB material was analysed by measuring fluorescence linked to HeLa cells after trypsin treatment under two alternative conditions. The “Mild” treatment (the regular protocol) used trypsin at 0.5 mg/ mL (final concentration) in HBSS for 3 min. The “Harsh” treatment was performed by adding trypsin 1 mg/ mL (final concentration), in HBSS for 15 min, and it had been previously designed to ensure the complete removal or externally attached protein [31]. The number of released cells in both cases was about 100 % of those present in the culture, and no significant differences were observed when used IB-decorated or naked PLA scaffolds

(65000±10897 for IB-decorated and 57500±17500 for naked respectively in the Mild treatment and 65000±23848 for IB-decorated and 65000±23848 for naked respectively in the Harsh treatment). Trypsin digestions were done at 37 °C in a humidified incubator at 5 % CO_2 and under gentle agitation conditions. After protein digestion cells were analyzed in a FACSCalibur system (BectonDickinson), using a 15 mW air-cooled argon-ion laser at 488 nm. Green fluorescence emission was measured with a 530/30 nm band pass filter. Data was acquired through CellQuest Pro software and further processed using the FlowJo 5.7.2 software.

Gene expression assay, RT-qPCR

NIH3t3 cells were cultured for 24 h on PLA scaffolds decorated with hFGF-2 IBs, and lysed for total RNA extraction with TRIreagent treatment (Sigma- Aldrich, MO, USA) according to manufacturer's instructions. RNA was then quantified in a nanodrop 2000c (thermo) and 250 ng of total RNA were reverse-transcribed using Sperscript III reverse transcriptase (Invitrogen S.A, Barcelona, Spain) and oligoDT (promega) as primer for cDNA extension. Real-time qPCR reaction was performed using a 1:5 dilution of the the cDNA in a Bio-Rad CFX96 RT-qPCR detection system with SYBR Green PCR Supermix (BioRad, Hercules, CA, USA). DNA amplification was detected by fluorescence incorporation after each qPCR cycle. The assay was carried out in order to determine the expression of the genes Angptl-4 and GAPDH. This last gene, due to its constitutive nature, was used to normalize *Angptl-4* expression. Gene expression was quantified by the comparative analysis of cycle-threshold procedure and it was represented as the relative value obtained when comparing cells cultured on IB-modified PLA scaffolds and on nude scaffolds. Sequences of the primers used in this assay were validated by the analysis of the melting curve as well as their efficiency curve. All samples were performed in triplicate. RNA controls gave no amplification signal. T-test was used to analyze variances between samples. Primer sequences were as follow: *Angptl*-4 forward: 5' CAGAGGGACCACTACAGTCCAACTA 3'; *Angptl*-

4 reverse: 5’ CACCCTGTCTCCAGTCAGTCAA 3’; *GAPDH* forward: 5’ACGGCACAGTCAAGGCCGAG 3’; *GAPDH* reverse: 5’CACCCTTCAAGTGGGCCCCG 3’

Culture of human mesenchymal stem cells

Purified human mesenchymal stem cells from bone marrow (hMSC) (CD105+, CD29+, $CD44^+$, $CD14^-$, $CD34^-$, $CD45^-$) were purchased from Cambrex Bio Science (Verviers, Belgium) and expanded in a defined medium (Cambrex Bio Science). Cells were maintained at 37ºC under 5 % CO_2 and 95 % air in a humidified incubator. hMSCs were seeded on PLA scaffolds in 12-well plates (4×10^5 cells/well) and cultured for 1 and 4 days. Cell viability was evaluated using the alamarBlue assay (Biosource, Nivelles, Belgium), which incorporates a nonfluorescent redox indicator that turns into a bright red fluorescent dye in response to metabolic activity.

Confocal imaging and IB scaffold penetration analysis

Polymer scaffolds were mounted on Mat-Teck culture dishes (Mat Teck Corp., Ashland, Massachusetts, United States) and images were taken with a TCS-SP5 confocal laser scanning microscope (Leica Microsystems, Heidelberg, Germany) using a Plan Apo 10x / 0.4 (dry) objective. GFP-based IBs were excited with an Argon laser (488 nm) and the emission was detected in the 500-560 nm range. Polymer matrices were collected in reflection mode with a 488 nm Argon laser and detected in the 480-495 nm range. Hoechst 33342 DNA labels (20 µg/ml, Molecular Probes) was excited with a blue diode (405 nm) and detected in the 415-460 nm range. To determine the 3D polymer microstructure and distribution of IBs, stacks of 40 to 100 sections were collected every 4 µm along the material’s thickness. Image processing was performed using the Imaris X64 v. 6.2.0 software (Bitplane; Zürich, Switzerland). Quantification of integrated fluorescence intensity (IF) of IBs versus scaffold depth was carried out using the Metamorph software package v. 5.0r1 (Universal Imaging Corporation Downington,

PA, USA). The images were segmented into foreground and background by setting a threshold, which was the same for all the samples. Blue self-fluorescence of the materials was minimized digitally.

Scanning electron microscopy

Scaffolds were mounted on copper stubs, and gold sputtered for scanning electron microscopy (SEM). The samples were observed with a JEOL JSM5410 scanning microscope under an acceleration tension of 10 kV.

On the other hand, purified IBs were deposited onto Track-Etched polycarbonate membranes with 0.2 µm pore size (Whatman, UK) and fixed in 2.5% (v/v) glutaraldehyde in 0.1 M PBS. Samples were then dehydrated and the CO_2 critical point was carried out by conventional procedures [27]. Samples were then mounted on adhesive carbon films and gold sputtered for observation in a Hitachi S-570 scanning microscope (Hitachi Ltd., Japan) at an accelerating voltage from 15kV to 20kV.

Results and discussion

VP1GFP IBs produced in a $ClpA^-$ background were fully fluorescent inside the producing bacteria (Figure 2 A) and once they had been isolated (Figure 2 B). They showed a smooth surface and a pseudo-spherical geometry with a diameter ranging between 300 and 400 nm (Figure 2 C).

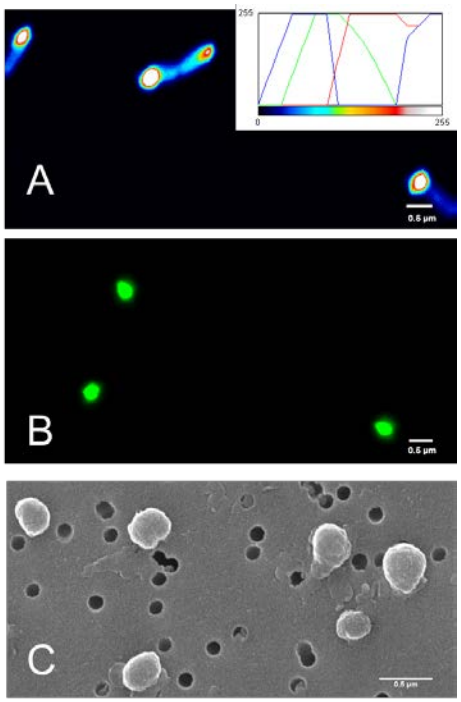

Figure 2. Geometry and bioactivity of IBs used in this study. A) Fluorescent IBs during biofabrication in ClpA$^-$ *E. coli* cells. Intensity of fluorescence ranged from low (dark colors) to high (white) (inset). B) Isolated ClpA$^-$ IBs upon cell disruption and washing. C) SEM images of ClpA$^-$ IBs showing spherical geometry and smooth surface. Size of the particles ranged between 300 and 400 nm.

The penetrability of these particles into PCL, PLA and CHT 3D scaffolds was tested with three different approaches: injection, dipping and dripping. We determined the fluorescence versus the distance from the scaffold surfaces upon decoration. In the three scaffolds, the highest emission were observed when the scaffolds were exposed to IBs through dipping (Figure 3 A), while injection was clearly the least favourable protocol under the tested conditions. Using dipping under our condition set, the amount of IBs peaked between 200 and 300 µm from the surface in PCL and PLA, while the other two methods did not permit the material to accumulate IBs above 100 µm. In CHT, the three approaches allowed the IBs to accumulate to similar depths (less than 100 µm), but again, dipping led to the retention of higher amounts of fluorescent material. The maximum depth to which the protein particles penetrated around 300 µm in all cases, and no significant levels of fluorescence were detected beyond this distance (Figure 3 A). Although the longitudinal penetrability of the protein particles in

CHT was clearly limited, the total amount of protein material that was embedded was slightly higher in this scaffold than in PCL or PLA (Figure 3 B). This difference is probably due to a higher solvent-material surface ratio being in the CHT scaffolds where the IBs can get in contact to the material surface more easily. Pore size, being the same in the three scaffolds, should not be a differential parameter. However, looking at the architecture of the 3 different matrices (Figure 1) a higher degree of cavity interconnection is apparent in PLA and PCL scaffolds comparing to CHT, in which the inner surfaces show a rather tubular organization. The amount of IBs retained by scaffolds was estimated for PLA, reaching around 37 µg of protein per piece.

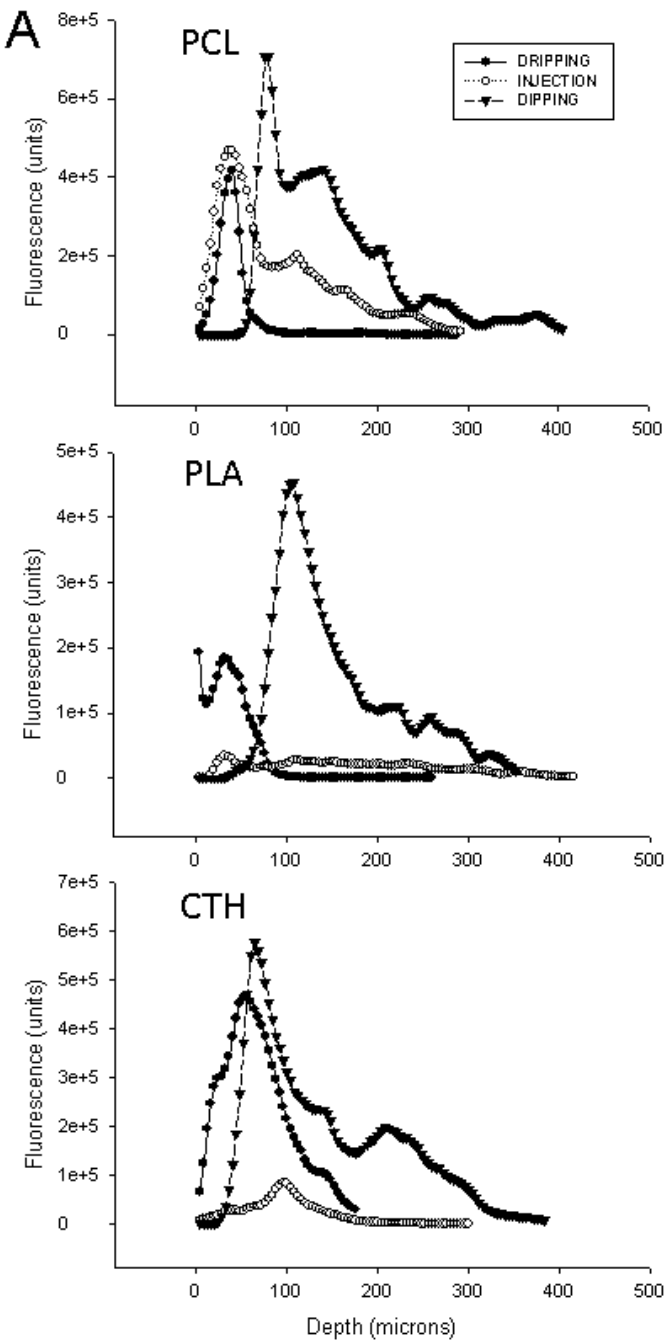
A
PCL
DRIPPING
INJECTION
DIPPING
Fluorescence (units)
8e+5
6e+5
4e+5
2e+5
0
0
100
200
300
400
500
PLA
5e+5
4e+5
3e+5
2e+5
1e+5
CTH
7e+5
6e+5
5e+5
Depth (microns)

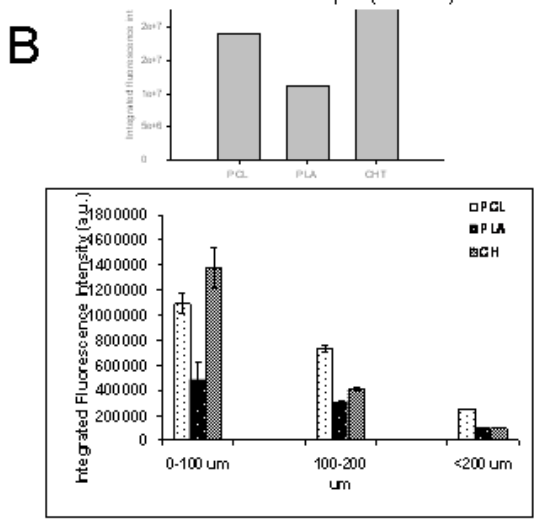
B
PCL
PLA
CHT
Integrated Fluorescence Intensity (a.u.)
1800000
1600000
1400000
1200000
1000000
800000
600000
400000
200000
0
0-100 um
100-200 um
<200 um

Figure 3. Penetrability of IBs into 3D scaffolds fabricated by alternative materials. A) Depth of fluorescence from the scaffolds' surface, upon decoration with ClpA^{-} IBs. The scaffolds were decorated by exposition to IBs through three alternative procedures (namely injection, dipping and dripping). B) Integrated fluorescence intensity upon dipping is comparatively shown in the three types of scaffolds.

This fact could explain the tendency of CHT scaffolds to accumulate particles near the scaffold surface. In addition, fine surface analysis of these scaffolds with DCM revealed that CHT owns the highest roughness values Ra, Rq and Rz (Figure 4, Table 1), probably due to its tubular organization, which could also contribute that IB particles accumulate near the surface. However, Rsk (skewness), which measures the symmetry of the deviation from a mean plane, was more negative on PCL and CHT than on PLA. This means that, comparatively, PLA has more peaks than valleys. On the other hand, PLA had the highest Rku values, a parameter that describes the probable density sharpness of the profile.

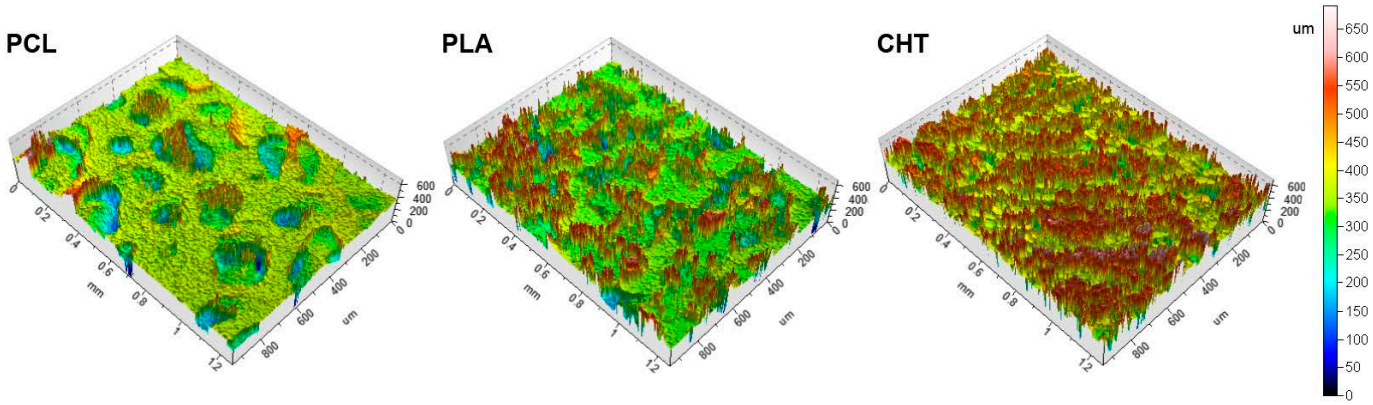

Figure 4. Topography images of the naked scaffolds obtained with the 3D Optical Surface Metrology System Leica DCM 3D used for a roughness study.

Table 1. Roughness values collected from a surface analysis.

Material

Parameter [a]	PCL	PLA	CHT
Ra	36.84±1.46 [b]	51.34±2.28	69.69±2.10
Rq	48.29±1.71	70.25±3.35	91.26±2.66
Rz	230.14±7.1	349.5±16.57	421.79±7.00
Rsk	-0.18±0.04	0.07±0.09	-0.16±0.09
Rku	4.33±0.09	5.42±0.14	3.63±0.15

[a] Values are given in microns.

[b] Data are the mean and standard error from 57 profiles of the five fields examined in each biomaterial.

Figure 5 shows 3D image reconstructions of the decorated materials in which both the particulate nature of the fluorescent material and the random distribution of the IBs can be observed. This indicates that the IBs are both mechanically and functionally stable during decoration and also that there are no massive aggregation, although moderate clustering was observed in CHT. In addition, the images indicated the absence of hot spots in the decoration process, and thus the entire solvent-exposed surface is available for IB adhesion.

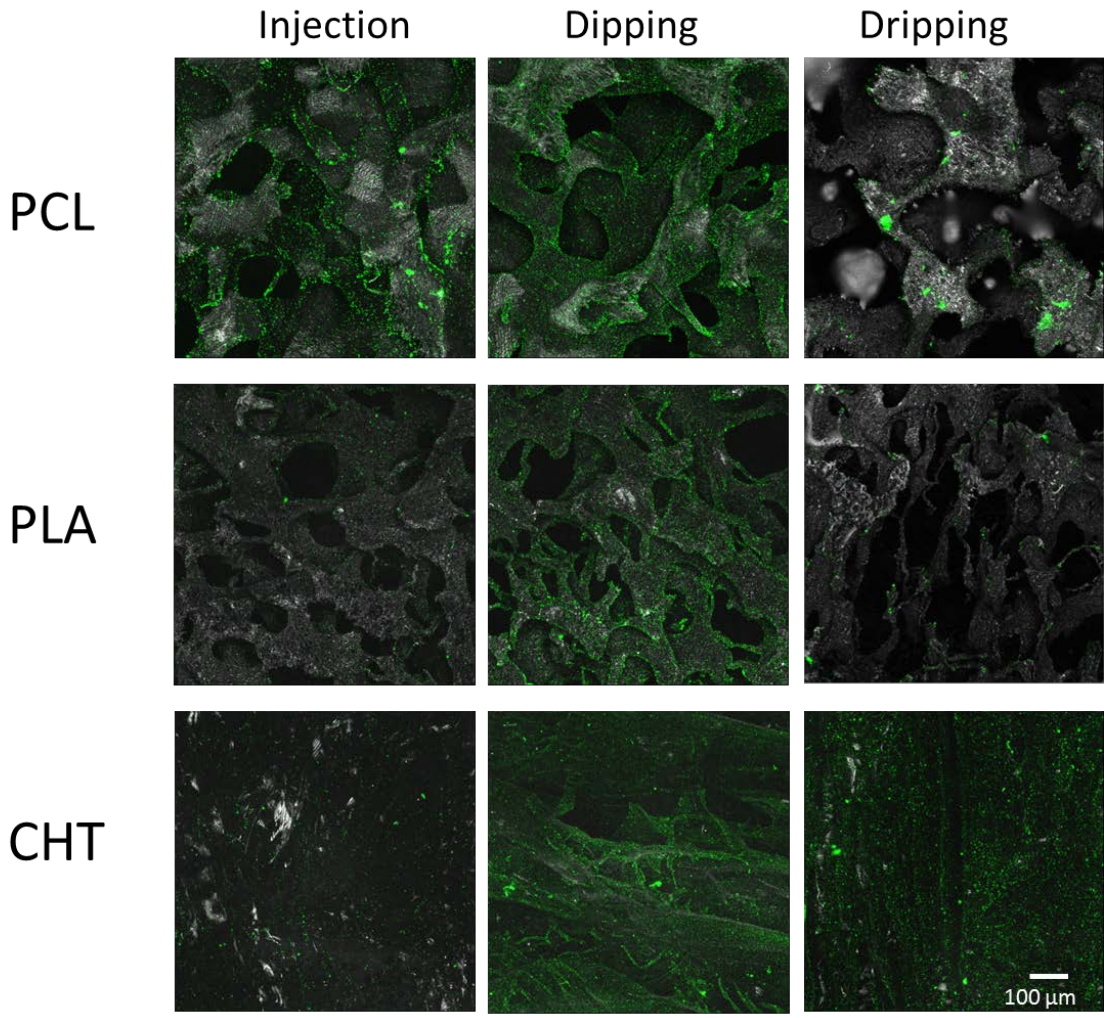

Figure 5. Decoration of 3D scaffolds with GFP IBs (green fluorescence) using different methods. Confocal projections of stacks of 70 to 90 sections with a z step of 4 µm. The scaffold is detected by reflection (grey). The magnification is equivalent in all panels.

When using IB-decorated 3D scaffolds for cell culture, cell penetrability and adhesion occurred correctly, and the cells distributed homogeneously through the inner surfaces of the scaffolds (Figure 6). No signs of toxicity promoted by IB decoration were observed in cells growing on any of these materials, as revealed by MTT assays (Figure 7 A), what prompted us to go further in the analysis of cell behavior in these materials. In 2D polystyrene surfaces, when non-treated for cell culture, IBs favored cell adhesion and mechanical stimulation of proliferation [17] (what was also observed on PLA surfaces (Figure 7 A), and we wondered at which extent this effect could be

also observed in 3D substrates. For that, 3D PLA scaffolds, that looked specially promising in the above experimental were decorated and tested in prolonged culture of hMSC, to anticipate a real application in a regenerative medicine context. As observed (Figure 7 B), IBs did not result toxic to the cells but in contrast, protein particles clearly favored cell proliferation and colonization of the substrate. This indicated that even in 3D environments, probably offering better conditions for mechanical stimuli than 2D surfaces, bacterial IBs are still able to favor colonization through topological enhancement of cell division, even of cells such as MSC whose culture require special care.

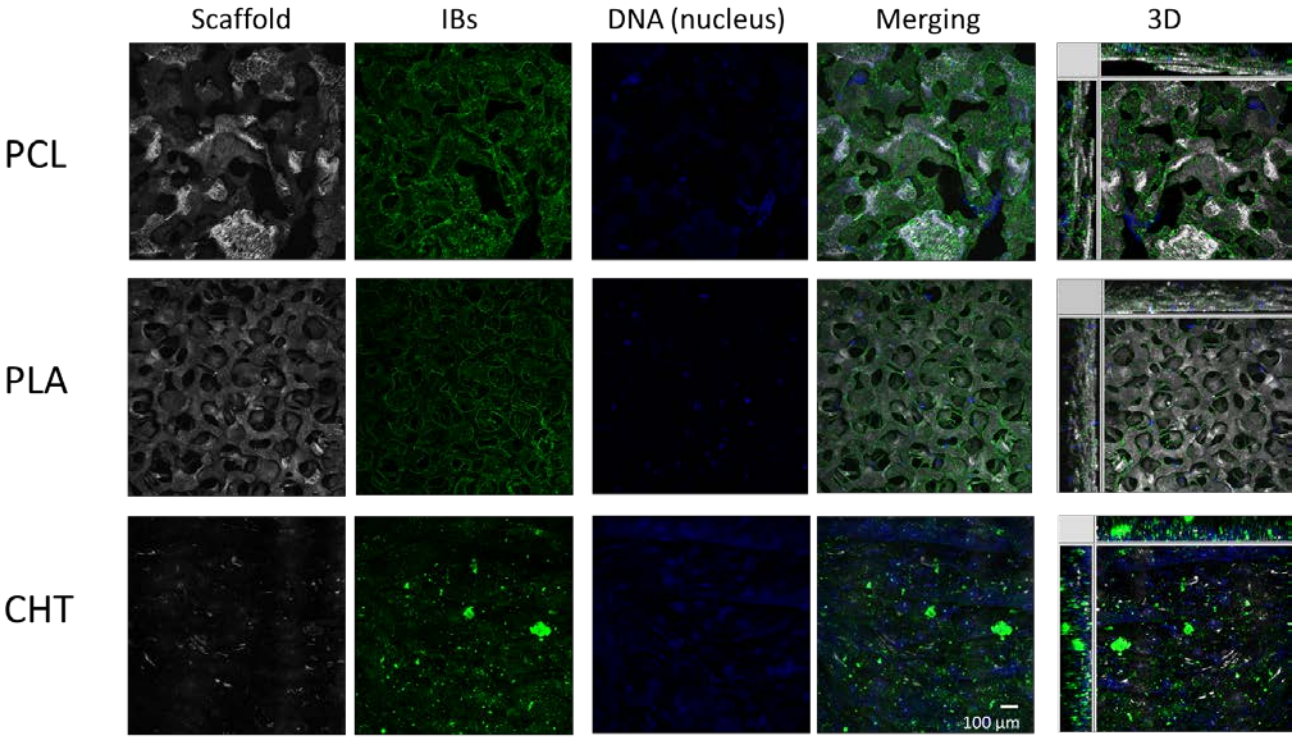

Figure 6. Cell colonization of IB-decorated 3D scaffolds. GFP IBs produce a green signal, scaffolds are detected by reflection (grey signal), and cell nuclei are labelled with Hoechst 33342 (blue signal). Confocal images are stacks of 70-90 sections. The magnification is equivalent in all panels.

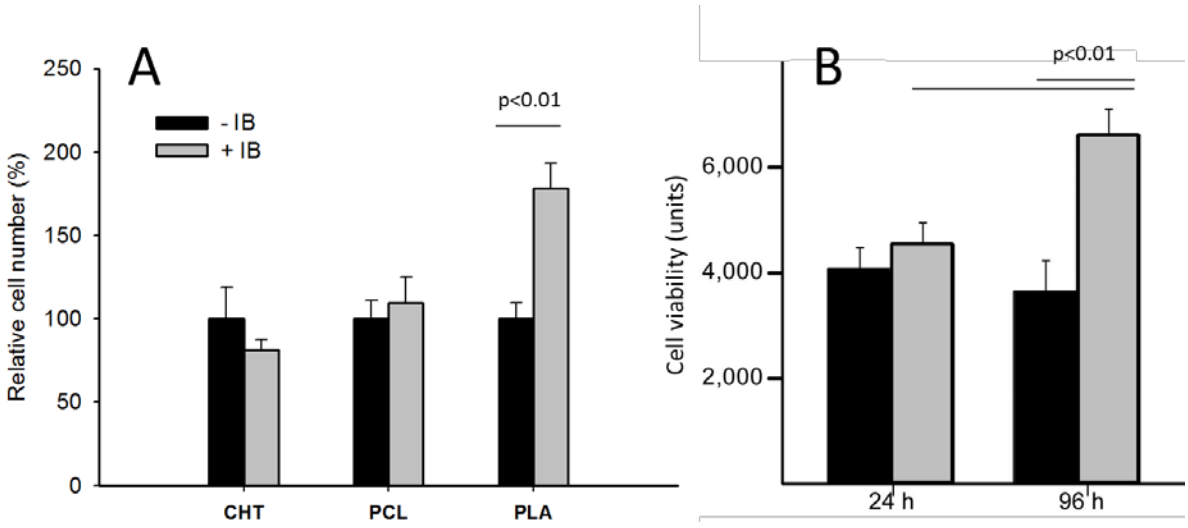

Figure 7. Cell growth of IB-decorated scaffolds. A) Relative number of 1BR3.G cells 48 hours after culture on flat CHT, PCL and PLA surfaces, naked (-) or decorated with IBs (+). B) Proliferation of hMSC cells in 3D PLA scaffolds at different times of culture, in absence (-) or in presence of IBs (+), given by units from the alamarBlue assay.

IBs show a natural penetrability into cellular membranes [24,27], offering promise as delivery systems of the proteins that form them [21,22,24,26]. In order to explore whether functional IB protein could be available to growing cells as presented in 3D scaffolds, we determined the percentage of cells incorporating green fluorescence upon culture on IB-decorated scaffolds for 24 hours. For that, we removed growing cells by a regular trypsin treatment (mild) or by a prolonged (harsh) exposure to the protease under conditions in which all the extracellular protein is removed [31]. In absence of IBs, no cells were observed to be fluorescent (Figure 8 A). However, an important fraction of cells become fluorescent when cultured on IB-decorated scaffolds (Figure 8 A). In PLA, that was further explored for IB-protein delivery, the fraction of fluorescent cells slightly decreases with time (Figure 8 B), concomitant with the increase in the cell number observed when culturing on this material (Figure 7 A). This fact strongly suggests that most of the IB material penetrates cultured cells early upon seeding, and that the functional protein from IBs remains available intracellularly for long time periods, sufficient in the tissue engineering context to provide biological

inputs to cultured cells. Internalization of IBs into cell membranes was further visually confirmed by 3D reconstructions of stacked confocal images in PLA-decorated cultures (Figure 8 C).

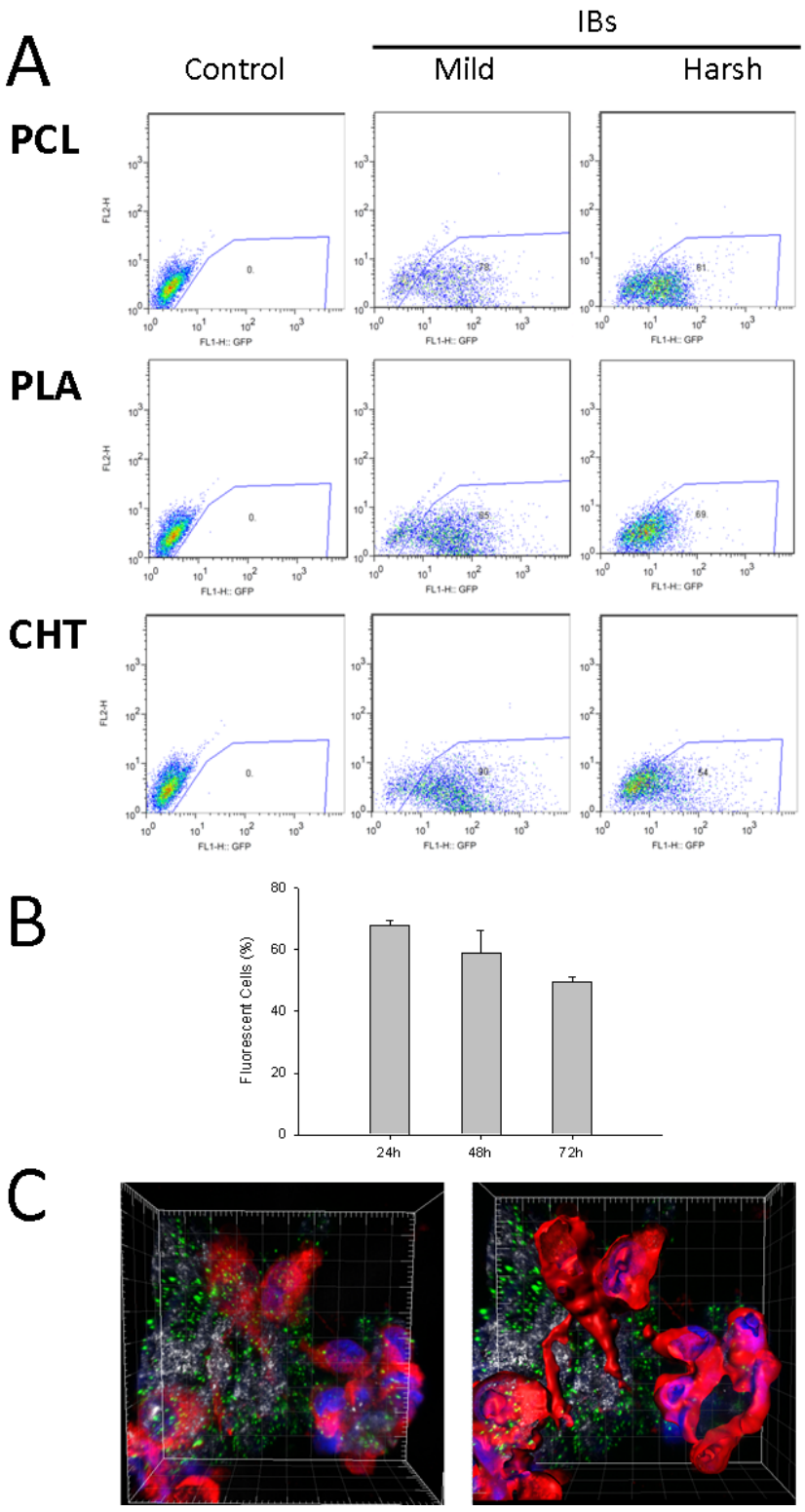

Figure 8. Penetration of IB material into cultured cells. A) Retention of green fluorescence by HeLa cells cultured on IB-decorated scaffolds after removing extracellular protein with Mild and Harsh Trypsin treatments. The column on the left shows HeLa cells cultured on naked scaffolds and removed by Harsh treatment. Y Axis corresponds to red fluorescence, represented to discriminate self-fluorescent cells. B) Time-dependence of the relative number of fluorescent cells growing on IB-decorated PLA scaffolds, as revealed by Harsh treatment. C ?????????

Upon statistics data analysis, we observed that between 80 and 90 % of cells retained fluorescence when detached by a mild trypsin treatment, irrespective of the material with which the scaffold is constructed (Figure 9 A). This indicates a homogenous dispersion of both IBs and cells on the materials' inner surfaces and also, an intimate contact of the membranes of the majority of cells with IBs, which promotes the retention of functional (fluorescent) GFP. In PCL, all the fluorescent cells have incorporated the fluorescence intracellular, while in PLA, a minor fraction of fluorescent cells retained GFP from IBs only associated to the external side of the cell membrane, and this material was removed by a harsh trypsin treatment (Figure 9 A). In CHT, about half of IB-exposed HeLa cells retained fluorescence only extracellularly (Figure 9 A), indicating that in this scaffold, internalization of IB protein was less efficient than in the other tested scaffolds. Its positive charge due to -NH3 groups (while PCL and PLA are negatively charged due to their superficial -COOH groups) might contribute to this differential protein uptake, as IBs exhibit a negative surface charge [32] and electrostatic retention by the material could partially prevent interaction with cells.

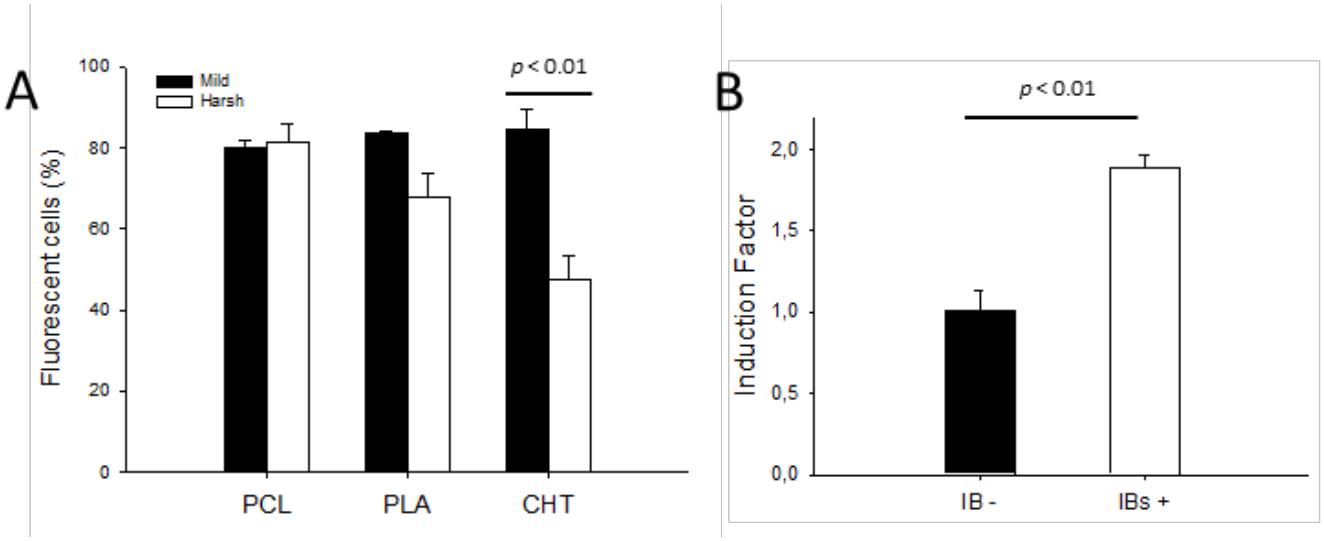

Figure 9. Cell penetrability of functional IB protein as released from IB-decorated 3D scaffolds. A) The fluorescent cell fraction resulting from subtracting *Harsh* from *Mild* data represents the efficiency of IB protein internalization. B) Induction of *Angptl-4* gene expression in PLA scaffolds decorated with FGF IBs. In both cases data were obtained in triplicate and statistically significant differences (p<0.01) are indicated.

Although these data obtained with a reporter fluorescent protein already indicated that protein uptake involved functional protein forms (fluorescent in this case), we wanted to confirm the occurrence of appropriate cells responses during the delivery of a biologically relevant protein. For that, we decorated 3D PLA scaffolds with IBs formed by the fibroblast growth factor 2 (FGF-2), that are fully active [33]. *Angptl-4* encoding the proangiogenic factor Angiopoietin-like 4 has been previously shown to be up-regulated in NIH3t3 cells in presence of FGF-2 [34]. As expected, cells cultured on scaffolds functionalized with FGF-2 IBs showed a 2-fold increase in the expression of *Angptl-4* (Figure 9 B), a result that fully confirms the cellular responsiveness of cells to protein factors released from IB-based 3D, functional cell culture platforms.

In summary, data presented here present 3D scaffolds formed by polymers as fully decoratable with active IBs, representing an interesting approach to the generation of

generic platforms for the multifactorial control of 3D cell culture. Among the tested materials, PLA was particularly good in allowing the penetration and retention of functional IBs up to around 300 µm in depth, being the dipping protocol as developed here the most proficient approach for IB decoration. In this material, growing cells internalized very efficiently functional protein from reporter IBs, what opens intriguing opportunities to design 3D hybrid matrices for the sustained release of functional proteins from IBs. Contrarily, CHT was only moderately penetrated by IBs and, in addition, only 50 % of the cells in contact with IBs efficiently internalized functional protein. Whether limited penetrability and moderate capabilities to allow intracellular protein delivery in this material are related events remains unclear, but apparently, both parameters are not mechanistically connected.

In the emerging field of tissue engineering, providing appropriate mechanical and biological stimuli is a way of mimicking the natural environment for the proliferation and eventual differentiation of mammalian cells [1,5,9]. Biodegradable materials, once structured in 3D scaffolds, are promising supports for both in vitro and in vivo generation of 3D tissue. Among the available functional, non-toxic amyloids [35-37], bacterial IBs are very efficient as nano- micro-particulate proteinaceous entities that, as they are fully compatible, can be used in biomedical interfaces such as those occurring in cell culture [16-18,20,27,38,39]. The sponge-like molecular organization of IBs [40], in which fibrils provide mechanical stability for embedding quasi-soluble proteins [22], provides a structural basis for the slow release of proteins inside contact cells, that take advantage of the natural membrane penetrability shown by IBs [24,27]. Due to the easy production, biocompatibility, functionality and tuneability of IBs [41], these particles have become a promising biomaterial for protein replacement and cellular therapies, through slow and sustained delivery of their building blocks [21].

Previous research on mammalian cell culture supported by IBs has been performed in 2D surfaces [20,33,42,43], which show a limited applicability in real tissue engineering problems. How IBs would perform in 3D scaffolds was fully unpredictable, and specially, the intimate interaction observed between IBs and cell membranes [24] could result impaired by the geometry of the scaffolds. Results presented here have shown a good penetrability of the protein particles in the tested materials (Figure 3) and an excellent performance in promoting cell proliferation, even of sensitive mesenchymal cells, in absence of toxicity (Figure 6). This was unexpected as 3D materials offer more mechanical stimuli to cell than their 2D counterparts. More importantly, protein drugs can be extracellularly and intracellularlly delivered from IB forms (Figure 7, 8), as in decorated scaffolds IBs can penetrate the cytosolic membrane and release active protein for biological activity. The unexpected ability of bacterial IBs to get embedded into or to cross mammalian cell membranes has been reported in detail elsewhere [24,27]. This fact is useful in regenerative medicine and could be used to design appropriate combinations of growth factors and other protein-based effectors, as importantly, essentially any protein of interest can be packaged as functional IBs [21]. Also, the principle of protein release from therapeutic IBs has been already proved, among others, for Hsp70 [24], keratin 14 (K14) [26], FGF-2 [27], leukemia inhibitory factor (LIF) [24], granulocyte-colony stimulating factor (G-CSF) [44] and catalase [24]. The potential offered by protein drug delivery from IB-decorated 3D scaffolds offer a versatile platform for the controlled release of growth factors and other protein drugs. Being not restricted to a specific protein or materials, it offers a plethora of opportunities and potential future applications in tissue engineering.

Finally, it can be envisaged that IBs, which are active once adsorbed on biopolymers, could be suitable for functionalizing hard materials such as ceramics and metals. Research into this area is now in progress.

Conclusions

3D scaffolds formed by PCL, PLA and CHT can be efficiently decorated by dipping (and less efficiently by dripping and injection) with bacterial IBs formed by functional protein, without loss of protein stability and biological activity. IBs reach deeper than 300 µm, homogeneously covering the inner surfaces of the materials. Decoration is especially competent in PCL. Upon cell culture in these scaffolds, about 80 % of cells are in contact with the IB protein, proving the absence of important empty surfaces upon decoration. In PCL, essentially all (100 %) these cells internalize functional IB protein, and internalization also occurs, at lesser extent, in PLA (around 85 %) and CHT (around 50 %). The study presented here support the decoration of polymeric 3D scaffolds as a way to generated hybrid scaffold-bioscaffold matrices for the robust delivery of biologically active protein drugs with sustained biological effects, formulated as bacterial IBs, to mammalian cells. This platform show promise in offering, at the same time, selected physical and biological stimuli in 3D approaches to tissue engineering.

Acknowledgments: We are indebted to MINECO (BFU2010-17450), AGAUR (2009SGR-0108) and CIBER de Bioingeniería, Biomateriales y Nanomedicina (CIBER-BBN, Spain) for funding our research on Inclusion bodies. CIBER-BBN is an initiative funded by the VI National R&D&i Plan *2008-2011*, Iniciativa Ingenio 2010, Consolider Program, CIBER Actions and financed by the Instituto de Salud Carlos III with assistance from the European Regional Development Fund. EGF is supported by the Programa Personal de Técnico de Apoyo (Modalidad Infraestructuras científico-tecnológicas, MICINN). We also thank technical assistance from the Servei de Cultius Cellulars, Producció d'Anticossos i Citometria (SCAC), and Servei de Microscòpia, both at the Universitat Autònoma de Barcelona (UAB). We are also indebted to the Protein Production Platform (CIBER-BBN) for helpful technical assistance and for

protein production and purification services (http://bbn.ciber-bbn.es/programas/plataformas/equipamiento). AV received an ICREA ACADEMIA award.

Conflict of interest

CV-A and AJC-F are linked to a company that produces and commercializes the 3D scaffolds used in this study. EG-F, EV and AV are co-inventors on two patents covering biomedical uses of IBs (WO2010131117 and WO2010076361). No other potential conflicts of interest have been identified.

Reference List

[1] E. Engel, A. Michiardi, M. Navarro, D. Lacroix, and J. A. Planell, Nanotechnology in regenerative medicine: the materials side, Trends Biotechnol., 26 (2008) 39-47.

[2] M. Peran, M. A. Garcia, E. Lopez-Ruiz, M. Bustamante, G. Jimenez, R. Madeddu, and J. A. Marchal, Functionalized nanostructures with application in regenerative medicine, Int. J. Mol. Sci., 13 (2012) 3847-3886.

[3] A. Ito and M. Kamihira, Tissue engineering using magnetite nanoparticles, Prog Mol. Biol. Transl. Sci., 104 (2011) 355-395.

[4] D. Khang, J. Carpenter, Y. W. Chun, R. Pareta, and T. J. Webster, Nanotechnology for regenerative medicine, Biomed. Microdevices., 12 (2010) 575-587.

[5] M. Navarro, A. Michiardi, O. Castano, and J. A. Planell, Biomaterials in orthopaedics, J. R. Soc. Interface, 5 (2008) 1137-1158.

[6] I. C. Bonzani, J. H. George, and M. M. Stevens, Novel materials for bone and cartilage regeneration, Curr. Opin. Chem. Biol., 10 (2006) 568-575.

[7] S. J. Hollister, Porous scaffold design for tissue engineering, Nat. Mater., 4 (2005) 518-524.

[8] M. J. Dalby, N. Gadegaard, R. Tare, A. Andar, M. O. Riehle, P. Herzyk, C. D. Wilkinson, and R. O. Oreffo, The control of human mesenchymal cell differentiation using nanoscale symmetry and disorder, Nat. Mater., 6 (2007) 997-1003.

[9] M. J. Dalby, Nanostructured surfaces: cell engineering and cell biology, Nanomed., 4 (2009) 247-248.

[10] A. Jaklenec, A. Hinckfuss, B. Bilgen, D. M. Ciombor, R. Aaron, and E. Mathiowitz, Sequential release of bioactive IGF-I and TGF-beta 1 from PLGA microsphere-based scaffolds, Biomaterials, 29 (2008) 1518-1525.

[11] S. Madduri, S. P. di, M. Papaloizos, D. Kalbermatten, and B. Gander, Effect of controlled co-delivery of synergistic neurotrophic factors on early nerve regeneration in rats, Biomaterials, 31 (2010) 8402-8409.

[12] S. H. Bhang, T. J. Lee, J. M. Lim, J. S. Lim, A. M. Han, C. Y. Choi, Y. H. Kwon, and B. S. Kim, The effect of the controlled release of nerve growth factor from collagen gel on the efficiency of neural cell culture, Biomaterials, 30 (2009) 126-132.

[13] N. A. Marcantonio, C. A. Boehm, R. J. Rozic, A. Au, A. Wells, G. F. Muschler, and L. G. Griffith, The influence of tethered epidermal growth factor on

connective tissue progenitor colony formation, Biomaterials, 30 (2009) 4629-4638.

[14] M. R. Doschak, C. M. Kucharski, J. E. Wright, R. F. Zernicke, and H. Uludag, Improved bone delivery of osteoprotegerin by bisphosphonate conjugation in a rat model of osteoarthritis, Mol. Pharm., 6 (2009) 634-640.

[15] A. Zieris, S. Prokoph, K. R. Levental, P. B. Welzel, M. Grimmer, U. Freudenberg, and C. Werner, FGF-2 and VEGF functionalization of starPEG-heparin hydrogels to modulate biomolecular and physical cues of angiogenesis, Biomaterials, 31 (2010) 7985-7994.

[16] E. Garcia-Fruitos, E. Vazquez, C. ez-Gil, J. L. Corchero, J. Seras-Franzoso, I. Ratera, J. Veciana, and A. Villaverde, Bacterial inclusion bodies: making gold from waste, Trends Biotechnol, 30 (2012) 65-70.

[17] J. Seras-Franzoso, C. Diez-Gil, E. Vazquez, E. Garcia-Fruitos, R. Cubarsi, I. Ratera, J. Veciana, and A. Villaverde, Bioadhesiveness and efficient mechanotransduction stimuli synergistically provided by bacterial inclusion bodies as scaffolds for tissue engineering, Nanomedicine (Lond), doi: 10.2217/NNM.11.83 (2011).

[18] E. Garcia-Fruitos, J. Seras-Franzoso, E. Vazquez, and A. Villaverde, Tunable geometry of bacterial inclusion bodies as substrate materials for tissue engineering, Nanotechnology., 21 (2010) 205101.

[19] C. Diez-Gil, S. Krabbenborg, E. Garcia-Fruitos, E. Vazquez, E. Rodriguez-Carmona, I. Ratera, N. Ventosa, J. Seras-Franzoso, O. Cano-Garrido, N. Ferrer-Miralles, A. Villaverde, and J. Veciana, The nanoscale properties of bacterial inclusion bodies and their effect on mammalian cell proliferation, Biomaterials, 31 (2010) 5805-5812.

[20] E. García-Fruitós, E. Rodríguez-Carmona, C. Díez-Gil, R. M. Ferraz, E. Vázquez, J. L. Corchero, M. Cano-Sarabia, I. Ratera, N. Ventosa, J. Veciana, and A. Villaverde, Surface Cell Growth Engineering Assisted by a Novel Bacterial Nanomaterial, Advanced Materials, 21 (2009) 4249-4253.

[21] A. Villaverde, E. Garcia-Fruitos, U. Rinas, J. Seras-Franzoso, A. Kosoy, J. L. Corchero, and E. Vazquez, Packaging protein drugs as bacterial inclusion bodies for therapeutic applications, Microb Cell Fact., 11 (2012) 76.

[22] O. Cano-Garrido, E. Rodriguez-Carmona, C. Diez-Gil, E. Vazquez, E. Elizondo, R. Cubarsi, J. Seras-Franzoso, J. L. Corchero, U. Rinas, I. Ratera, N. Ventosa, J. Veciana, A. Villaverde, and E. Garcia-Fruitos, Supramolecular organization of protein-releasing functional amyloids solved in bacterial inclusion bodies, Acta Biomater., (2012).

[23] A. Villaverde, Bacterial inclusion bodies: an emerging platform for drug delivery and cell therapy, Nanomedicine. (Lond), 7 (2012) 1277-1279.

[24] E. Vazquez, J. L. Corchero, J. F. Burgueno, J. Seras-Franzoso, A. Kosoy, R. Bosser, R. Mendoza, J. M. Martinez-Lainez, U. Rinas, E. Fernandez, L. Ruiz-

Avila, E. Garcia-Fruitos, and A. Villaverde, Functional Inclusion Bodies Produced in Bacteria as Naturally Occurring Nanopills for Advanced Cell Therapies, Adv. Mater., 24 (2012) 1742-1747.

[25] García-Fruitós E, Vazquez E, Corchero JL, and Villaverde A. Use of inclusion bodies as therapeutic agents. IB2010/001330[WO2010131117A1]. 18-11-2010.
Ref Type: Patent

[26] M. Liovic, M. Ozir, Z. A. Bedina, S. Peternel, R. Komel, and T. Zupancic, Inclusion bodies as potential vehicles for recombinant protein delivery into epithelial cells, Microb Cell Fact., 11 (2012) 67.

[27] Seras-Franzoso J, Peebo K, Corchero JL, Tsimbouri, P. M., Unzueta U, Rinas, U., Dalby, M., Vazquez E, García-Fruitós, Elena, and Villaverde A. A nanostructured bacterial bio-scaffold for the sustained bottom-up delivery of protein drugs. Nanomedicine (Lond) . 2013.
Ref Type: In Press

[28] J. G. Thomas and F. Baneyx, Roles of the *Escherichia coli* small heat shock proteins IbpA and IbpB in thermal stress management: comparison with ClpA, ClpB, and HtpG In vivo, J Bacteriol, 180 (1998) 5165-5172.

[29] E. Garcia-Fruitos, M. Martinez-Alonso, N. Gonzalez-Montalban, M. Valli, D. Mattanovich, and A. Villaverde, Divergent Genetic Control of Protein Solubility and Conformational Quality in *Escherichia coli*, J. Mol. Biol., 374 (2007) 195-205.

[30] E. Rodriguez-Carmona, O. Cano-Garrido, J. Seras-Franzoso, A. Villaverde, and E. Garcia-Fruitos, Isolation of cell-free bacterial inclusion bodies, Microb. Cell Fact., 9 (2010) 71.

[31] J. P. Richard, K. Melikov, E. Vives, C. Ramos, B. Verbeure, M. J. Gait, L. V. Chernomordik, and B. Lebleu, Cell-penetrating peptides. A reevaluation of the mechanism of cellular uptake, J. Biol. Chem., 278 (2003) 585-590.

[32] J. Seras-Franzoso, C. ez-Gil, E. Vazquez, E. Garcia-Fruitos, R. Cubarsi, I. Ratera, J. Veciana, and A. Villaverde, Bioadhesiveness and efficient mechanotransduction stimuli synergistically provided by bacterial inclusion bodies as scaffolds for tissue engineering, Nanomedicine (Lond), 7 (2012) 79-93.

[33] J. Seras-Franzoso, K. Peebo, J. L. Corchero, P. M. Tsimbouri, U. Unzueta, U. Rinas, M. J. Dalby, E. Vazquez, E. Garcia-Fruitos, and A. Villaverde, A nanostructured bacterial bioscaffold for the sustained bottom-up delivery of protein drugs, Nanomedicine (Lond), (2013).

[34] N. Quarto, K. D. Fong, and M. T. Longaker, Gene profiling of cells expressing different FGF-2 forms, Gene, 356 (2005) 49-68.

[35] S. Mankar, A. Anoop, S. Sen, and S. K. Maji, Nanomaterials: amyloids reflect their brighter side, Nano Rev., 2 (2011).

[36] S. K. Maji, M. H. Perrin, M. R. Sawaya, S. Jessberger, K. Vadodaria, R. A. Rissman, P. S. Singru, K. P. Nilsson, R. Simon, D. Schubert, D. Eisenberg, J. Rivier, P. Sawchenko, W. Vale, and R. Riek, Functional amyloids as natural storage of peptide hormones in pituitary secretory granules, Science, 325 (2009) 328-332.

[37] S. K. Maji, D. Schubert, C. Rivier, S. Lee, J. E. Rivier, and R. Riek, Amyloid as a depot for the formulation of long-acting drugs, PLoS Biol., 6 (2008) e17.

[38] C. Diez-Gil, S. Krabbenborg, E. Garcia-Fruitos, E. Vazquez, E. Rodriguez-Carmona, I. Ratera, N. Ventosa, J. Seras-Franzoso, O. Cano-Garrido, N. Ferrer-Miralles, A. Villaverde, and J. Veciana, The nanoscale properties of bacterial inclusion bodies and their effect on mammalian cell proliferation, Biomaterials, 31 (2010) 5805-5812.

[39] E. Rodriguez-Carmona and A. Villaverde, Nanostructured bacterial materials for innovative medicines, Trends Microbiol., 18 (2010) 423-430.

[40] S. Peternel, S. Jevsevar, M. Bele, V. Gaberc-Porekar, and V. Menart, New properties of inclusion bodies with implications for biotechnology, Biotechnol. Appl. Biochem., 49 (2008) 239-246.

[41] E. Garcia-Fruitos, E. Vazquez, C. Diez-Gil, J. L. Corchero, J. Seras-Franzoso, I. Ratera, J. Veciana, and A. Villaverde, Bacterial inclusion bodies: making gold from waste, Trends Biotechnol, doi:10.1016/j.tibtech.2011.09.003 (2011).

[42] J. Seras-Franzoso, P. M. Tsimbouri, K. V. Burgess, U. Unzueta, E. Garcia-Fruitos, E. Vazquez, A. Villaverde, and M. J. Dalby, Topographically targeted osteogenesis of mesenchymal stem cells stimulated by inclusion bodies attached to polycaprolactone surfaces, Nanomedicine (Lond), (2013).

[43] J. Seras-Franzoso, C. Diez-Gil, E. Vazquez, E. Garcia-Fruitos, R. Cubarsi, I. Ratera, J. Veciana, and A. Villaverde, Bioadhesiveness and efficient mechanotransduction stimuli synergistically provided by bacterial inclusion bodies as scaffolds for tissue engineering, Nanomedicine (Lond), 7 (2012) 79-93.

[44] S. Jevsevar, V. Gaberc-Porekar, I. Fonda, B. Podobnik, J. Grdadolnik, and V. Menart, Production of nonclassical inclusion bodies from which correctly folded protein can be extracted, Biotechnol. Prog., 21 (2005) 632-639.